

Singular-value statistics of directed random graphs

J. A. Méndez-Bermúdez

*Instituto de Física, Benemérita Universidad Autónoma de Puebla, Puebla 72570, Mexico
Escuela de Física, Facultad de Ciencias, Universidad Nacional Autónoma de Honduras, Honduras*

R. Aguilar-Sánchez

Facultad de Ciencias Químicas, Benemérita Universidad Autónoma de Puebla, Puebla 72570, Mexico

Singular-value statistics (SVS) has been recently presented as a random matrix theory tool able to properly characterize non-Hermitian random matrix ensembles [PRX Quantum **4**, 040312 (2023)]. Here, we perform a numerical study of the SVS of the non-Hermitian adjacency matrices \mathbf{A} of directed random graphs, where \mathbf{A} are members of diluted real Ginibre ensembles. We consider two models of directed random graphs: Erdős-Rényi graphs and random regular graphs. Specifically, we focus on the ratio r between nearest neighbor singular values and the minimum singular value λ_{\min} . We show that $\langle r \rangle$ (where $\langle \cdot \rangle$ represents ensemble average) can effectively characterize the transition between mostly isolated vertices to almost complete graphs, while the probability density function of λ_{\min} can clearly distinguish between different graph models.

PACS numbers:

I. PRELIMINARIES

There is already a vast number of applications of Random Matrix Theory (RMT) measures and techniques to the study and characterization of complex graphs and networks. The general idea of RMT is that given a matrix representing a system or process, if that system or process is complex enough, the corresponding matrix can be substituted by an ensemble of random matrices having the symmetries of the original matrix (see e.g. [1]). Then, luckily, such a random matrix ensemble may allow for an analytical (or a phenomenological) statistical approach that may describe the *universal* properties of the original complex system or of the family of complex systems represented by matrices sharing the same symmetries. Otherwise, a statistical numerical study of the random matrix ensemble may also provide useful information about the corresponding complex system. In this respect, the application of RMT to complex graphs and networks is quite straightforward through their matrix representations (see e.g. [2]): adjacency matrix, Laplacian matrix, incidence matrix, etc., and variants of them.

Among the wide amount of available studies of graphs and networks from a RMT perspective we can mention that: (i) the density of states of random graphs has been approached by generalizing the semicircle law (see e.g. [3–5]), (ii) spectral properties of several models of random graphs have been characterized by the use of the nearest neighbor spacing distribution, the singular value decomposition, and the ratio between nearest- and next-to-nearest neighbor eigenvalues, and other RMT measures (see e.g. [5–21]), (iii) eigenvector properties of several models of random graphs have been characterized by the use of Shannon entropies and inverse participation ratios (see e.g. [15–25]), while (iv) scattering and transport properties of tight-binding random graphs have been studied by means of the effective non-Hermitian Hamiltonian approach (see e.g. [26, 27]).

Specifically, among the models of graphs and networks which have been approached with the above measures and techniques we have: Erdős-Rényi random graphs (see e.g. [6–8, 13, 25]), small-world networks (see e.g. [6–8]), scale free networks (see e.g. [6–8]), random geometric graphs (see e.g. [15, 16, 21]), bipartite graphs (see e.g. [17]), mutualistic graphs (see e.g. [18]), multilayer and multiplex networks (see e.g. [10, 11, 19, 23, 24]), etc.

A. Singular-value statistics

For a matrix \mathbf{A} , its singular values λ are defined as the square roots of the eigenvalues of $\mathbf{A}\mathbf{A}^\dagger$ or $\mathbf{A}^\dagger\mathbf{A}$, where, as usual, \mathbf{A}^\dagger is the conjugate transpose of \mathbf{A} . For a Hermitian matrix, i.e. $\mathbf{A}^\dagger = \mathbf{A}$, the singular values reduce to the absolute values of the eigenvalues of \mathbf{A} .

In Ref. [28], with the focus on open quantum systems, the statistical properties of singular values for all the 38-fold symmetry classes of non-Hermitian random matrices was extensively investigated. There, it was shown that singular-value statistics (SVS) can be used as an effective measure for chaos and nonintegrability in open quantum systems. Specifically, the SVS of small random matrices was analytically derived for the ratio between nearest neighbor singular values and for the minimum singular value; both were shown to describe well the SVS of large random matrices.

Given that the adjacency matrices \mathbf{A} of directed random graphs and networks are non-Hermitian, it is straightforward to think on the SVS as a tool to study the spectral properties of \mathbf{A} by computing the real singular values of $\mathbf{A}\mathbf{A}^\dagger$ instead of working with the complex eigenvalues of \mathbf{A} . Indeed, that is the purpose of this work: Here we study the SVS of the non-Hermitian adjacency matrices of directed random graphs. Since for real matrices, as the ones we consider here, the conjugate transpose is just the transpose $\mathbf{A}^\dagger = \mathbf{A}^T$, then, in what follows, the

SVS concerns the spectra of $\mathbf{A}\mathbf{A}^T$.

In the next Section we characterize the real spectra of the Hermitian matrix $\mathbf{A}\mathbf{A}^T$ and, as a reference, we also characterize the complex spectra of the non-Hermitian adjacency matrix \mathbf{A} by computing, respectively, the average value of the ratio between nearest neighbor singular values $r_{\mathbb{R}}$ and the average value of the ratio between nearest- and next-to-nearest neighbor eigenvalues $r_{\mathbb{C}}$, which are defined as follows.

On the one hand, given the real ordered spectrum $\lambda_1 > \lambda_2 > \dots > \lambda_{n-1} > \lambda_n$, the k -th ratio $r_{\mathbb{R}}^k$ reads as [29, 30]

$$r_{\mathbb{R}}^k = \frac{\min(\lambda_{k+1} - \lambda_k, \lambda_k - \lambda_{k-1})}{\max(\lambda_{k+1} - \lambda_k, \lambda_k - \lambda_{k-1})}. \quad (1)$$

Here, $r_{\mathbb{R}} \in [0, 1]$. On the other hand, given the complex spectrum $\{\lambda_k\}$ the k -th ratio $r_{\mathbb{C}}^k$ reads as [31]

$$r_{\mathbb{C}}^k = \frac{|\lambda_k^{NN} - \lambda_k|}{|\lambda_k^{NNN} - \lambda_k|}, \quad (2)$$

where λ_k^{NN} and λ_k^{NNN} are, respectively, the nearest and the next-to-nearest neighbors of λ_k in \mathbb{C} . Note that, as well as $r_{\mathbb{R}}$, $r_{\mathbb{C}} \in [0, 1]$. Moreover, note that $r_{\mathbb{C}}$ can also be computed for real spectra.

It is relevant to mention that the singular values of certain adjacency matrices of specific deterministic graphs have already been studied in Ref. [32]. Also, there is an analytical study of the distribution of the minimum singular value of the randomly weighted adjacency matrices of directed Erdős-Rényi graphs in the regime of large average degree $\langle k \rangle \gg 1$ [33]. However, we are not aware of any statistical (numerical) study of the the singular values of random graphs.

B. Models of directed random graphs

We consider two models of directed random graphs G : the directed Erdős-Rényi graph (dERG) model and the directed random regular graph (dRRG) model. In the dERG model, $G(n, p)$ has n vertices and each directed edge appears independently with probability $p \in (0, 1]$. While the graphs of the dRRG model, $G(n, \rho)$, consist of n vertices uniformly and independently distributed on the unit square where two vertices are connected by a directed edge if their euclidean distance is smaller than the connection radius $\rho \in (0, \sqrt{2}]$.

C. The randomly-weighted adjacency matrix

Once a random directed graph is constructed, $G(n, p)$ or $G(n, \rho)$, its binary adjacency matrix is weighted with random variables (including self loops) as follows:

$$[\mathbf{A}]_{uv} = \begin{cases} \epsilon_{uu} & \text{if } u = v, \\ \epsilon_{uv} & \text{if } u \rightarrow v, \\ 0 & \text{otherwise.} \end{cases} \quad (3)$$

Here, we choose ϵ_{uv} as statistically-independent random variables drawn from a normal distribution with zero mean and variance one, $\epsilon_{uv} \sim \mathcal{N}(0, 1)$. Evidently, since G is directed, $\epsilon_{uv} \neq \epsilon_{vu}$; thus, \mathbf{A} is non-Hermitian. Note that \mathbf{A} is a member of a *diluted* real Ginibre ensemble (RGE) [34]; the RGE consists of random $n \times n$ matrices formed from independent and identically distributed standard Gaussian entries. Then, for a complete graph, when $p = 1$ in the dERG model or $\rho = \sqrt{2}$ in the dRRG model, \mathbf{A} becomes a member of the RGE. Notice, in addition, that when $p = 0$ or $\rho = 0$, i.e. for isolated vertices, \mathbf{A} becomes a member of the Poisson Ensemble (PE) [35]; that is, \mathbf{A} is a diagonal real random matrix. Thus, a transition from the PE to the RGE is expected when increasing p from zero to one in the dERG model and when increasing ρ from zero to $\sqrt{2}$ in the dRRG model. We note that some spectral properties of the RGE were reported in Ref. [36]. Also, diluted RGEs were already considered in Refs. [20] and [21] as models of randomly weighted adjacency matrices of dERGs and dRRGs, respectively.

II. NUMERICAL RESULTS

In what follows we use exact numerical diagonalization to obtain the eigenvalues λ_k ($k = 1, \dots, n$) of ensembles of adjacency matrices \mathbf{A} and ensembles of the corresponding matrix products $\mathbf{A}\mathbf{A}^T$ for both $G(n, p)$ and $G(n, \rho)$.

A. Ratio between nearest neighbor singular values

In Fig. 1(a) we present the average ratio between nearest neighbor singular values $\langle r_{\mathbb{R}}(\mathbf{A}\mathbf{A}^T) \rangle$ (see dot-dashed lines) of dERGs as a function of the probability p . In Fig. 1(b) we also show $\langle r_{\mathbb{R}}(\mathbf{A}\mathbf{A}^T) \rangle$ (also as dot-dashed lines) but of dRRGs as a function of the connection radius ρ . For both graph models we used graphs of five sizes: $n = 100, 200, 400, 800$, and 1600 . Indeed, we have verified that for these sizes the graph models are already in the large n limit; see Appendix A for a small-graph size analysis. For comparison purposes, in Figs. 1(a) and 1(b) we include $\langle r_{\mathbb{C}}(\mathbf{A}\mathbf{A}^T) \rangle$ (full lines) and, as a reference, we also plot $\langle r_{\mathbb{C}}(\mathbf{A}) \rangle$ (dashed lines); i.e. the ratio between nearest and next-to-nearest complex eigenvalues of the non-Hermitian adjacency matrix \mathbf{A} . In fact, $\langle r_{\mathbb{C}}(\mathbf{A}) \rangle$ for dERGs and dRRGs has already been reported in Refs. [20] and [21], respectively.

To ease the comparison of the average ratios we conveniently normalize them as

$$\langle \bar{r}_{\mathbb{R}}(\mathbf{A}\mathbf{A}^T) \rangle \equiv \frac{\langle r_{\mathbb{R}}(\mathbf{A}\mathbf{A}^T) \rangle - \langle r_{\mathbb{R}} \rangle_{(\text{PE})(\text{PE})^T}}{\langle r_{\mathbb{R}} \rangle_{(\text{RGE})(\text{RGE})^T} - \langle r_{\mathbb{R}} \rangle_{(\text{PE})(\text{PE})^T}}, \quad (4)$$

$$\langle \bar{r}_{\mathbb{C}}(\mathbf{A}\mathbf{A}^T) \rangle \equiv \frac{\langle r_{\mathbb{C}}(\mathbf{A}\mathbf{A}^T) \rangle - \langle r_{\mathbb{C}} \rangle_{(\text{PE})(\text{PE})^T}}{\langle r_{\mathbb{C}} \rangle_{(\text{RGE})(\text{RGE})^T} - \langle r_{\mathbb{C}} \rangle_{(\text{PE})(\text{PE})^T}} \quad (5)$$

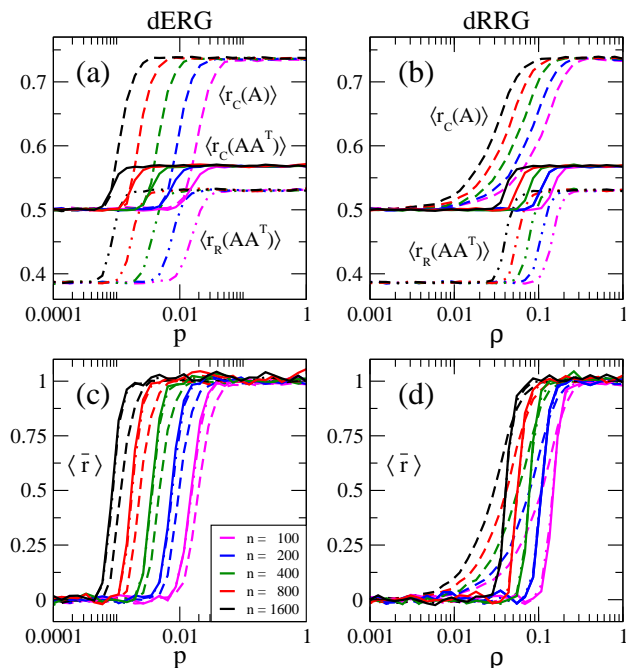


FIG. 1: Average ratios $\langle r_{\mathbb{R}}(\mathbf{A}\mathbf{A}^T) \rangle$ (dot-dashed lines), $\langle r_{\mathbb{C}}(\mathbf{A}\mathbf{A}^T) \rangle$ (full lines) and $\langle r_{\mathbb{C}}(\mathbf{A}) \rangle$ (dashed lines) of (a) directed Erdős-Rényi graphs (of size n) as a function of the probability p and (b) directed random regular graphs (of size n) as a function of the connection radius ρ . Normalized ratios $\langle \bar{r}_{\mathbb{R}}(\mathbf{A}\mathbf{A}^T) \rangle$, $\langle \bar{r}_{\mathbb{C}}(\mathbf{A}\mathbf{A}^T) \rangle$ and $\langle \bar{r}_{\mathbb{C}}(\mathbf{A}) \rangle$ [see Eqs. (4), (5) and (6), respectively] for (c) directed Erdős-Rényi graphs [same curves of panel (a)] and (d) directed random regular graphs [same curves of panel (c)]. All averages are computed over 10^6 ratios.

and

$$\langle \bar{r}_{\mathbb{C}}(\mathbf{A}) \rangle \equiv \frac{\langle r_{\mathbb{C}}(\mathbf{A}) \rangle - \langle r_{\mathbb{C}} \rangle_{\text{PE}}}{\langle r_{\mathbb{C}} \rangle_{\text{RGE}} - \langle r_{\mathbb{C}} \rangle_{\text{PE}}}; \quad (6)$$

so they all take values between zero and one. The reference values used in Eqs. (4-6), corresponding to the PE and the RGE, are reported in Table I. Then, in Figs. 1(c,d) we plot the normalized ratios $\langle \bar{r}_{\mathbb{R}}(\mathbf{A}\mathbf{A}^T) \rangle$, $\langle \bar{r}_{\mathbb{C}}(\mathbf{A}\mathbf{A}^T) \rangle$ and $\langle \bar{r}_{\mathbb{C}}(\mathbf{A}) \rangle$ for both dERGs and dRRGs, respectively.

From Fig. 1 we can conclude that all three ratios can effectively characterize the transition between the regime of mostly isolated vertices, where $\langle \bar{r}_{\mathbb{R}}(\mathbf{A}\mathbf{A}^T) \rangle \approx \langle \bar{r}_{\mathbb{C}}(\mathbf{A}\mathbf{A}^T) \rangle \approx \langle \bar{r}_{\mathbb{C}}(\mathbf{A}) \rangle \approx 0$, and the regime of mostly connected graphs, where $\langle \bar{r}_{\mathbb{R}}(\mathbf{A}\mathbf{A}^T) \rangle \approx \langle \bar{r}_{\mathbb{C}}(\mathbf{A}\mathbf{A}^T) \rangle \approx$

TABLE I: Reference average values of the ratios $r_{\mathbb{R}}$ and $r_{\mathbb{C}}$ for the random adjacency matrices used in this work. To compute the averages, the spectra of 10^3 adjacency matrices of size $n = 1000$ were used.

	PE	(PE)(PE) ^T	RGE	(RGE)(RGE) ^T
$\langle r_{\mathbb{R}} \rangle$	–	0.386	–	0.531
$\langle r_{\mathbb{C}} \rangle$	0.500	0.500	0.737	0.569

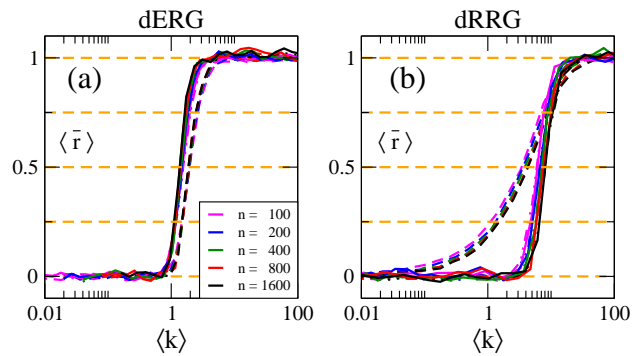


FIG. 2: Normalized ratios $\langle \bar{r}_{\mathbb{R}}(\mathbf{A}\mathbf{A}^T) \rangle$, $\langle \bar{r}_{\mathbb{C}}(\mathbf{A}\mathbf{A}^T) \rangle$ and $\langle \bar{r}_{\mathbb{C}}(\mathbf{A}) \rangle$ as a function of the average degree $\langle k \rangle$ for (a) directed Erdős-Rényi graphs [same curves of Fig. 1(c)] and (b) directed random regular graphs [same curves of Fig. 1(d)]. Horizontal dashed lines in (a,b) mark the values of $\langle \bar{r} \rangle$ used to compute the PDFs reported in Fig. 3.

$\langle \bar{r}_{\mathbb{C}}(\mathbf{A}) \rangle \approx 1$. Moreover, notice that

$$\langle \bar{r}_{\mathbb{C}}(\mathbf{A}\mathbf{A}^T) \rangle \approx \langle \bar{r}_{\mathbb{R}}(\mathbf{A}\mathbf{A}^T) \rangle \quad (7)$$

for both graph models; i.e. the dot-dashed curves and the full curves in Figs. 1(c,d) fall one on top the other (for a give graph size n and a given graph model). This means that $\langle r_{\mathbb{R}}(\mathbf{A}\mathbf{A}^T) \rangle$ and $\langle r_{\mathbb{C}}(\mathbf{A}\mathbf{A}^T) \rangle$, once normalized, provide the same information; so they can be used indistinguishably on real spectra.

It is also instructive to plot the ratios as a function of the average degree $\langle k \rangle$, see Fig. 2; so we can better contrast both graph models. Here, we can clearly see that the transition from almost isolated vertices to almost complete graphs is quite sharp when characterized by $\langle r_{\mathbb{R}}(\mathbf{A}\mathbf{A}^T) \rangle$ and $\langle r_{\mathbb{C}}(\mathbf{A}\mathbf{A}^T) \rangle$ for both graph models. However, when using $\langle r_{\mathbb{C}}(\mathbf{A}) \rangle$, the transition is much wider for dRRGs than for dERGs. This may indicate that $\langle r_{\mathbb{C}}(\mathbf{A}) \rangle$ may be a better tool to distinguish different graph models than $\langle r_{\mathbb{R}}(\mathbf{A}\mathbf{A}^T) \rangle$ or $\langle r_{\mathbb{C}}(\mathbf{A}\mathbf{A}^T) \rangle$. Anyway, it could be possible to distinguish between the graph models we are exploring here by using $\langle r_{\mathbb{R}}(\mathbf{A}\mathbf{A}^T) \rangle$ or $\langle r_{\mathbb{C}}(\mathbf{A}\mathbf{A}^T) \rangle$: Note that the transition for dERGs starts at a smaller value of $\langle k \rangle$ ($\langle k \rangle \approx 1$) as compared to dRRGs ($\langle k \rangle \approx 4$).

For completeness, we now inspect the probability density functions (PDFs) of the ratios $r_{\mathbb{R}}(\mathbf{A}\mathbf{A}^T)$, $r_{\mathbb{C}}(\mathbf{A}\mathbf{A}^T)$ and $r_{\mathbb{C}}(\mathbf{A})$. Moreover, for a meaningful comparison, we compute the PDFs at fixed values of the normalized ratios. Specifically, we choose five values of $\langle \bar{r} \rangle$, as indicated by the horizontal dashed lines in Figs. 2(a,b): $\langle \bar{r} \rangle \approx 0, 1/4, 1/2, 3/4, 1$. We note that there are many possible values of p [ρ] that produce $\langle \bar{r} \rangle \approx 0$ and 1 for dERGs [dRRGs]; here and below we set $p = 0.0001$ [$\rho = 0.001$] and $p = 0.5$ [$\rho = 1$] to get $\langle \bar{r} \rangle \approx 0$ and 1, respectively.

Then, in the upper panels of Fig. 3 we report the probability density function of the ratio $r_{\mathbb{R}}(\mathbf{A}\mathbf{A}^T)$. Each panel corresponds to a fixed average ratio $\langle \bar{r} \rangle$. Note that each panel in Fig. 3 contains six histograms: three of dERGs (in light colors) and three of dRRGs (in dark colors) of

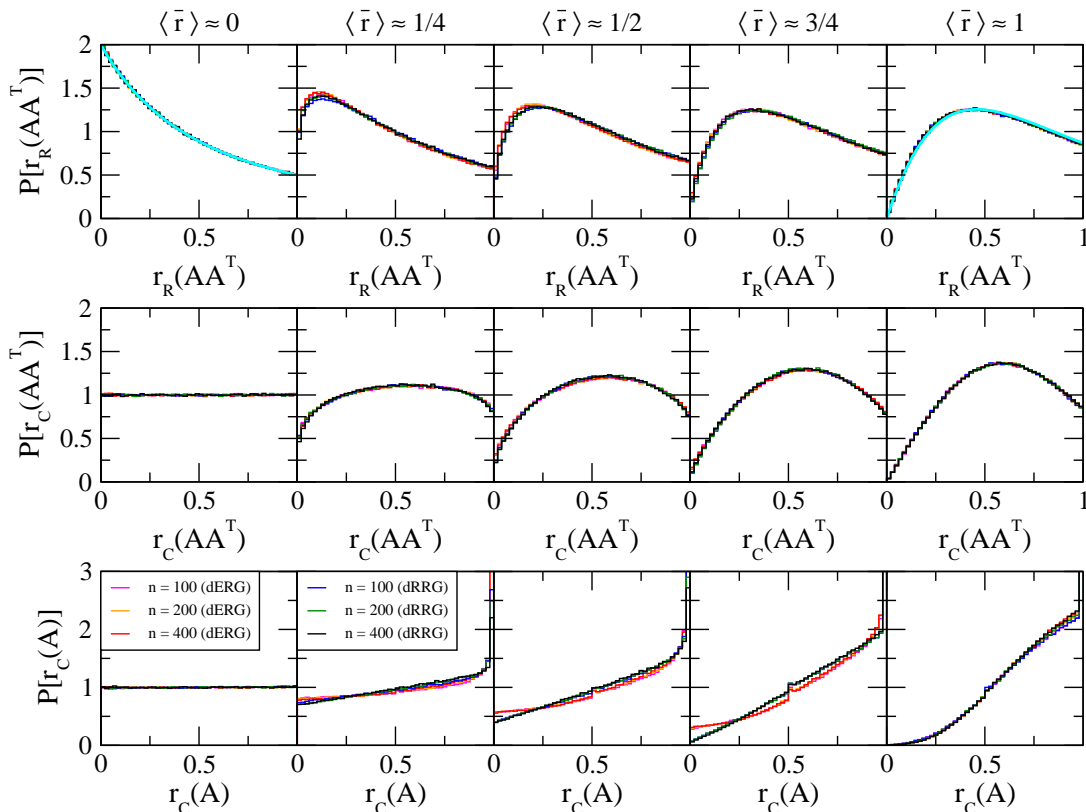


FIG. 3: Probability density function of the ratios $r_{\mathbb{R}}(\mathbf{A}\mathbf{A}^T)$ (upper panels), $r_{\mathbb{C}}(\mathbf{A}\mathbf{A}^T)$ (middle panels) and $r_{\mathbb{C}}(\mathbf{A})$ (lower panels) of directed Erdős-Rényi graphs and directed random regular graphs of size n . Each histogram was constructed from the ratios of 10^6 random graphs. The normalized rations $\langle \bar{r} \rangle$ are fixed in each column. Full cyan lines in upper-left and upper-right panels are Eqs. (8) and (9), respectively.

different sizes. As expected, once the average ratio $\langle \bar{r} \rangle$ is fixed, $P[r_{\mathbb{R}}(\mathbf{A}\mathbf{A}^T)]$ does not depend on the graph size, and in this case, neither on the graph model. Also, as expected [28], when $\langle \bar{r} \rangle \approx 0$, $P[r_{\mathbb{R}}(\mathbf{A}\mathbf{A}^T)]$ is well reproduced by the RMT prediction for the PE [30]

$$P_{\text{PE}}(r_{\mathbb{R}}) = \frac{2}{(1+r_{\mathbb{R}})^2}, \quad (8)$$

see the cyan curve in the upper-left panel; while for $\langle \bar{r} \rangle \approx 1$, $P[r_{\mathbb{R}}(\mathbf{A}\mathbf{A}^T)]$ corresponds to the RMT prediction for the GOE [30]

$$P_{\text{GOE}}(r_{\mathbb{R}}) = \frac{27}{4} \frac{r_{\mathbb{R}} + r_{\mathbb{R}}^2}{(1+r_{\mathbb{R}}+r_{\mathbb{R}}^2)^{5/2}}, \quad (9)$$

see the cyan curve in the upper-right panel.

In Fig. 3 we also plot $P[r_{\mathbb{C}}(\mathbf{A}\mathbf{A}^T)]$ (middle panels) and $P[r_{\mathbb{C}}(\mathbf{A})]$ (lower panels). It is interesting to note that, as well as for $P[r_{\mathbb{R}}(\mathbf{A}\mathbf{A}^T)]$, once the average ratio is fixed, $P[r_{\mathbb{C}}(\mathbf{A}\mathbf{A}^T)]$ can not distinguish between different graph models; i.e. all histograms in the upper and middle panels of Fig. 3 fall one on top of the other. However, $P[r_{\mathbb{C}}(\mathbf{A})]$ can indeed distinguish between dERGs and dRRGs: Notice that the histograms corresponding to different graph models follow slightly different shapes;

see the difference between light-color (dERGs) and dark-color (dRRGs) histograms in the lower panels of Fig. 3, specifically when $0 < \langle \bar{r} \rangle < 1$. This is in accordance with the observations made in Fig. 2: While $\langle r_{\mathbb{R}}(\mathbf{A}\mathbf{A}^T) \rangle$ and $\langle r_{\mathbb{C}}(\mathbf{A}\mathbf{A}^T) \rangle$ are not able to easily distinguish between the two graph models, $\langle r_{\mathbb{C}}(\mathbf{A}) \rangle$ can.

B. Minimum singular value λ_{\min}

Now we explore the statistics of the minimum singular value λ_{\min} . We start by plotting, in Figs. 4(a) and 4(b), the ratio $\langle \lambda_{\min}^2 \rangle / \langle \lambda_{\min} \rangle^2$ for dERGs (as a function of the probability p) and for dRRGs (as a function of the connection radius ρ), respectively. From Fig. 4 we observe, by increasing the connectivity in both graph models, the transition of $\langle \lambda_{\min}^2 \rangle / \langle \lambda_{\min} \rangle^2$ from the PE value $\langle \lambda_{\min}^2 \rangle_{\text{PE}} / \langle \lambda_{\min} \rangle_{\text{PE}}^2 = 2$ [28] to the RGE value, that we report as $\langle \lambda_{\min}^2 \rangle_{\text{RGE}} / \langle \lambda_{\min} \rangle_{\text{RGE}}^2 \approx 1.6$. We note that our value for $\langle \lambda_{\min}^2 \rangle_{\text{RGE}} / \langle \lambda_{\min} \rangle_{\text{RGE}}^2$ is larger than that analytically computed in Ref. [28] for 2×2 matrices; this difference is due to the graph sizes we consider here, that could be considered as large sizes. However, as it is clear from this figure, the PE-to-RGE transition

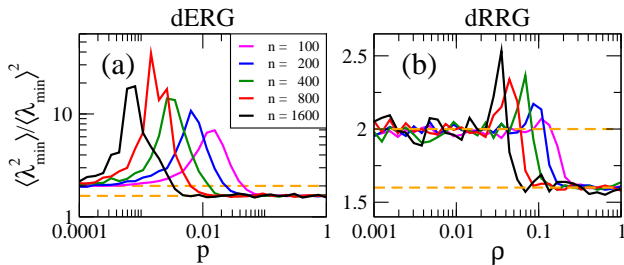


FIG. 4: (a) [(b)] $\langle \lambda_{\min}^2 \rangle / \langle \lambda_{\min} \rangle^2$ of directed Erdős-Rényi graphs of size n as a function of the probability p [of directed random regular graphs of size n as a function of the connection radius ρ]. Orange dashed lines correspond to $\langle \lambda_{\min}^2 \rangle_{\text{PE}} / \langle \lambda_{\min} \rangle_{\text{PE}}^2 = 2$ [28] and $\langle \lambda_{\min}^2 \rangle_{\text{RGE}} / \langle \lambda_{\min} \rangle_{\text{RGE}}^2 \approx 1.6$. The averages are computed over $10^6/n$ minimum singular values.

is not smooth and for increasing connectivity the ratio $\langle \lambda_{\min}^2 \rangle / \langle \lambda_{\min} \rangle^2$ first increases, reaches a maximum and then decreases approaching the RGE value. What is even more remarkable is that for dERGs the maximal values that $\langle \lambda_{\min}^2 \rangle / \langle \lambda_{\min} \rangle^2$ can reach are about one order of magnitude larger than those for dRRGs. So, the ratio $\langle \lambda_{\min}^2 \rangle / \langle \lambda_{\min} \rangle^2$ can indeed distinguish between both graph models.

Finally, in Fig. 5 we report the probability density function of the minimum singular value λ_{\min} normalized to $\langle \lambda_{\min} \rangle$, $P(\lambda_{\min} / \langle \lambda_{\min} \rangle)$, of dERGs and dRRGs. As in Fig. 3, here each panel of Fig. 5 contains six histograms: three of dERGs (in light colors) and three of dRRGs (in dark colors) of different sizes. Also each panel corresponds to a fixed average ratio $\langle \bar{r} \rangle$ (as indicated on top of the panels). As expected, we observe the PE-to-RGE transition of $P(\lambda_{\min} / \langle \lambda_{\min} \rangle)$ for increasing connectivity in both graph models, here parametrized by $\langle \bar{r} \rangle$; see the limiting PDFs in the left and right panels of Fig. 5. However, for intermediate values of $\langle \bar{r} \rangle$, see the central panels of Fig. 5, $P(\lambda_{\min} / \langle \lambda_{\min} \rangle)$ is clearly different for different graph models: Notice that the histograms for dERGs (in light colors) do not coincide with those for dRRGs (in dark colors). Thus, as well as the ratio $\langle \lambda_{\min}^2 \rangle / \langle \lambda_{\min} \rangle^2$, $P(\lambda_{\min} / \langle \lambda_{\min} \rangle)$ can clearly distinguish between both graph models.

III. DISCUSSION AND CONCLUSIONS

We have performed a numerical study of the singular-value statistics (SVS) of the non-Hermitian, randomly weighted, adjacency matrices \mathbf{A} of two models of ran-

dom graphs: directed Erdős-Rényi graphs (dERGs) and directed random regular graphs (dRRGs).

We have computed the ratios r between nearest neighbor singular values and the minimum singular values λ_{\min} . We have shown that the average values of r and λ_{\min} as well as the corresponding PDFs can effectively characterize the transition between mostly isolated vertices (Poisson Ensemble (PE) regime) to almost complete graphs (Real Ginibre Ensemble (RGE) regime); see Figs. 2 to 5. However, in contrast to $\langle r \rangle$ and $P(r)$, both $\langle \lambda_{\min} \rangle$ and $P(\lambda_{\min})$ can clearly distinguish between the two graph models; see Figs. 4 and 5. This means that even though both graph models produce adjacency matrices \mathbf{A} which are members of diluted RGEs which are structurally very similar, such that most average topological quantities can not distinguish them (see e.g. [37]), the minimum singular values can.

In addition, there may be other RMT tools that could also be incorporated in the study and characterization of directed graphs and networks, such as the hard-edge statistics, recently discussed in Ref. [38].

Appendix A: Small graphs

In order to make sure that the results reported in the main text are already in the large graph-size limit, here we perform a study of small graphs. Then, in Fig. 6 we plot $\langle r_{\mathbb{R}}(\mathbf{A}\mathbf{A}^T) \rangle$, $\langle r_{\mathbb{C}}(\mathbf{A}\mathbf{A}^T) \rangle$ and $\langle r_{\mathbb{C}}(\mathbf{A}) \rangle$ of dERGs (left panels) and dRRGs (right panels) of small size n . In all panels we include, as horizontal dashed lines, the expected values of the ratios for the PE (lower lines) and the RGE (upper lines) for large graphs, as given in Table I.

From Fig. 6 we can clearly see that while $\langle r_{\mathbb{R}}(\mathbf{A}\mathbf{A}^T) \rangle$ reproduces both the PE and the RGE values expected for large graphs already for graph sizes of the order of $n = 10$, see red curves in panels (a,b), for $\langle r_{\mathbb{C}}(\mathbf{A}\mathbf{A}^T) \rangle$ and $\langle r_{\mathbb{C}}(\mathbf{A}) \rangle$ larger graphs sizes are needed. We concluded that to avoid small-graph size effects, for all ratios, we need to set $n \geq 50$ at least. Therefore, for the calculations in the main text we consider $n \geq 100$.

Acknowledgements

J.A.M.-B. thanks support from CONAHCyT-Fronteras (Grant No. 425854) and VIEP-BUAP (Grant No. 100405811-VIEP2024), Mexico.

-
- [1] G. Akemann, J. Baik, and P. DiFrancesco, *The Oxford Handbook of Random Matrix Theory* (Oxford University Press, 2015).
 [2] E. Estrada, *The Structure of Complex Networks: Theory*

- and Applications (Oxford University Press, 2011).
 [3] R. Kühn, *Spectra of random stochastic matrices and relaxation in complex systems*, *Europhys. Lett.* **109** 60003 (2015).

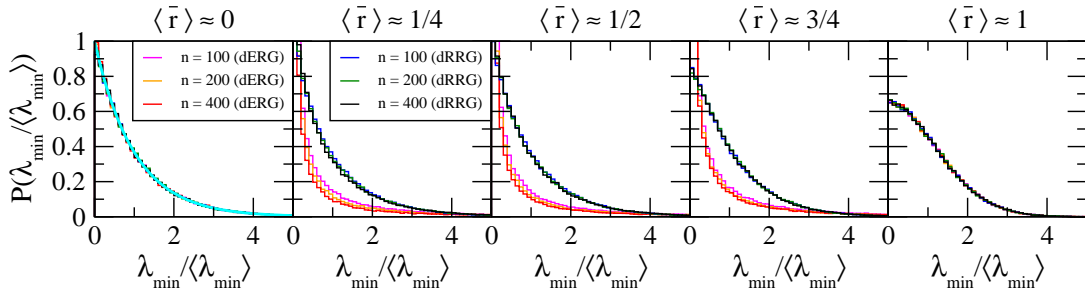


FIG. 5: Probability density function of the minimum singular value λ_{\min} normalized to $\langle \lambda_{\min} \rangle$ of directed Erdős-Rényi graphs and directed random regular graphs of size n . Each histogram was constructed from the ratios of 10^5 random graphs. The normalized ratios $\langle \bar{r} \rangle$ are fixed in each panel. Full cyan line in left panel is $P_{PE}(\lambda_{\min}/\langle \lambda_{\min} \rangle) = \exp[-\lambda_{\min}/\langle \lambda_{\min} \rangle]$ [28].

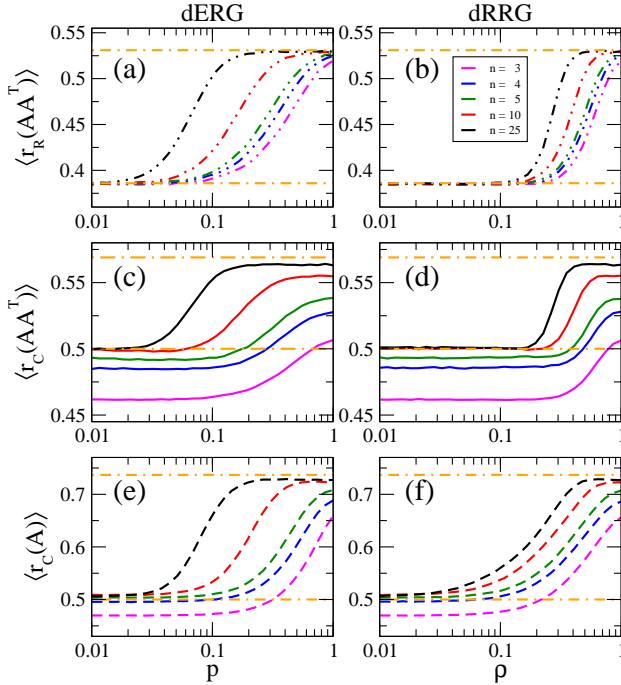


FIG. 6: Average ratios (a) $\langle r_{\mathbb{R}}(\mathbf{A}\mathbf{A}^T) \rangle$, (b) $\langle r_{\mathbb{C}}(\mathbf{A}\mathbf{A}^T) \rangle$ and (c) $\langle r_{\mathbb{C}}(\mathbf{A}) \rangle$ of directed Erdős-Rényi graphs (of small size n) as a function of the probability p . Average ratios (d) $\langle r_{\mathbb{R}}(\mathbf{A}\mathbf{A}^T) \rangle$, (e) $\langle r_{\mathbb{C}}(\mathbf{A}\mathbf{A}^T) \rangle$ and (f) $\langle r_{\mathbb{C}}(\mathbf{A}) \rangle$ of directed random regular graphs (of small size n) as a function of the connection radius ρ . All averages are computed over 10^6 ratios. Horizontal dashed lines are the expected values of the ratios for the PE (lower lines) and the RGE (upper lines) for large graphs, as given in Table I.

[4] A. Bazzani, A Random Matrix Theory approach to Complex Networks, PhD Thesis, Universita di Bologna (2019).
 [5] C. Sarkar and S. Jalan, Spectral properties of complex networks, *Chaos* **28**, 102101 (2018).
 [6] J. N. Bandyopadhyay and S. Jalan, Universality in complex networks: Random matrix analysis, *Phys. Rev. E* **76**, 026109 (2007).
 [7] S. Jalan and J. N. Bandyopadhyay, Random matrix analysis of complex networks, *Phys. Rev. E* **76**, 046107 (2007).

[8] S. Jalan and J. N. Bandyopadhyay, Random matrix analysis of network Laplacians, *Physica A* **387**, 667–674 (2008).
 [9] S. Jalan and J. N. Bandyopadhyay, Randomness of random networks: A random matrix analysis, *Europhys. Lett.* **87**, 48010 (2009).
 [10] T. Raghav and S. Jalan, Random matrix analysis of multiplex networks, *Physica A* **586**, 126457 (2022).
 [11] T. Raghav and S. Jalan, Spacing ratio statistics of multiplex directed networks, *New J. Phys.* **25**, 053012 (2023).
 [12] A. Mishra, T. Raghav, and S. Jalan, Eigenvalue ratio statistics of complex networks: Disorder versus randomness, *Phys. Rev. E* **105**, 064307 (2022).
 [13] J. A. Mendez-Bermudez, A. Alcazar-Lopez, A. J. Martinez-Mendoza, F. A. Rodrigues, and T. K. DM. Peron, Universality in the spectral and eigenfunction properties of random networks, *Phys. Rev. E* **91**, 032122 (2015).
 [14] G. Torres-Vargas, R. Fossion, and J. A. Mendez-Bermudez, Normal mode analysis of spectra of random networks, *Physica A* **545**, 123298 (2020).
 [15] L. Alonso, J. A. Mendez-Bermudez, A. Gonzalez-Melendrez, and Y. Moreno, Weighted random-geometric and random-rectangular graphs: Spectral and eigenfunction properties of the adjacency matrix, *J. Complex Networks* **6**, 753 (2018).
 [16] R. Aguilar-Sanchez, J. A. Mendez-Bermudez, F. A. Rodrigues, and J. M. Sigarreta-Almira, Topological versus spectral properties of random geometric graphs, *Phys. Rev. E* **102**, 042306 (2020).
 [17] C. T. Martinez-Martinez, J. A. Mendez-Bermudez, Y. Moreno, J. J. Pineda-Pineda, and J. M. Sigarreta, Spectral and localization properties of random bipartite graphs, *Chaos Soliton Fract. X* **3**, 100021 (2019).
 [18] C. T. Martinez-Martinez, J. A. Mendez-Bermudez, T. Peron, and Y. Moreno, Statistical properties of mutualistic-competitive random networks, *Chaos Soliton Fract.* **153**, 111504 (2021).
 [19] J. A. Mendez-Bermudez, G. Ferraz-de-Arruda, F. A. Rodrigues, and Y. Moreno, Scaling properties of multilayer random networks, *Phys. Rev. E* **96**, 012307 (2017).
 [20] T. Peron, B. M. F. de Resende, F. A. Rodrigues, L. da F. Costa, and J. A. Mendez-Bermudez, Spacing ratio characterization of the spectra of directed random networks, *Phys. Rev. E* **102**, 062305 (2020).
 [21] K. Peralta-Martinez and J. A. Mendez-Bermudez, Directed random geometric graphs: structural and spectral

- properties, *J. Phys. Complex.* **4**, 015002 (2023).
- [22] S. Jalan, N. Solymosi, G. Vattay and B. Li, Random matrix analysis of localization properties of gene coexpression network, *Phy. Rev. E* **81**, 046118 (2010).
- [23] S. Jalan and P. Pradhan, Localization of multilayer networks by optimized single-layer rewiring, *Phy. Rev. E* **97**, 042314 (2018).
- [24] Universality of eigenvector delocalization and the nature of the SIS phase transition in multiplex networks, G. Ferraz-de-Arruda, J. A. Mendez-Bermudez, F. A. Rodrigues, and Y. Moreno, *J. Stat. Mech.* 103405 (2020).
- [25] L. F. Cugliandolo, G. Schehr, M. Tarzia, D. Venturelli, Multifractal phase in the weighted adjacency matrices of random Erdős-Rényi graphs preprint arXiv:2404.06931.
- [26] A. J. Martinez-Mendoza, A. Alcazar-Lopez, and J. A. Mendez-Bermudez, Scattering and transport properties of tight-binding random networks, *Phys. Rev. E* **88**, 122126 (2013).
- [27] A. M. Martinez-Arguello, K. B. Hidalgo-Castro, and J. A. Mendez-Bermudez, Universal insulating-to-metallic crossover in tight-binding random geometric graphs, preprint arXiv:2310.03936.
- [28] K. Kawabata, Z. Xiao, T. Ohtsuki, and R. Shindou, Singular-value statistics of non-Hermitian random matrices and open quantum systems, *PRX Quantum* **4**, 040312 (2023).
- [29] V. Oganessian and D. A. Huse, Localization of interacting fermions at high temperature, *Phys. Rev. B* **75**, 155111 (2007).
- [30] Y. Atas, E. Bogomolny, O. Giraud, and G. Roux, Distribution of the ratio of consecutive level spacings in random matrix ensembles, *Phys. Rev. Lett.* **110**, 084101 (2013).
- [31] L. Sá, P. Ribeiro, and T. Prosen, Complex spacing ratios: A signature of dissipative quantum chaos, *Phys. Rev. X* **10**, 021019 (2020).
- [32] T. Powell, The Singular Values of the Exponentiated Adjacency Matrixes of Broom-Tree Graphs, HMC Senior Theses (2006).
- [33] Z. Che and P. Lopatto, Universality of the least singular value for sparse random matrices preprint arXiv:1711.00580.
- [34] J. Ginibre, Statistical ensembles of complex, quaternion, and real matrices, *J. Math. Phys.* **6**, 440 (1965).
- [35] M. L. Mehta, *Random Matrices* (Elsevier, 2004).
- [36] P. J. Forrester and T. Nagao, Eigenvalue statistics of the real ginibre ensemble, *Phys. Rev. Lett.* **99**, 050603 (2007).
- [37] R. Aguilar-Sanchez, J. A. Mendez-Bermudez, J. M. Rodriguez, and J. M. Sigarreta, Normalized Sombor indices as complexity measures of random networks, *Entropy* **23**, 976 (2021).
- [38] Z. Xiao, R. Shindou, and K. Kawabata, Universal hard-edge statistics of non-Hermitian random matrices, preprint arXiv:2401.05044.